NJC

Accepted Manuscript

This is an *Accepted Manuscript*, which has been through the Royal Society of Chemistry peer review process and has been accepted for publication.

Accepted Manuscripts are published online shortly after acceptance, before technical editing, formatting and proof reading. Using this free service, authors can make their results available to the community, in citable form, before we publish the edited article. We will replace this *Accepted Manuscript* with the edited and formatted *Advance Article* as soon as it is available.

You can find more information about *Accepted Manuscripts* in the Information for Authors.

Please note that technical editing may introduce minor changes to the text and/or graphics, which may alter content. The journal's standard Terms & Conditions and the Ethical guidelines still apply. In no event shall the Royal Society of Chemistry be held responsible for any errors or omissions in this *Accepted Manuscript* or any consequences arising from the use of any information it contains.

ROYAL SOCIETY OF CHEMISTRY

www.rsc.org/njc

New Journal of Chemistry

ARTICLE

Received 00th January 20xx,

Accepted 00th January 20xx

DOI: 10.1039/x0xx00000x

www.rsc.org/

Investigation of magnetic and electrochemical sensing properties of novel $Ba_{1/3}Mn_{1/3}Co_{1/3}Fe_2O_4$ nanoparticles

Nadir S.E. Osman[a1]*, Neeta Thapliyal[b1], Thomas Moyo[a1] and Rajshekhar Karpoormath[b1]*

Novel $Ba_{1/3}Mn_{1/3}Co_{1/3}Fe_2O_4$ nanoparticles were successfully synthesized using glycol thermal route. The X-ray diffraction study confirmed well-defined spinel phase structure of the sample. The microstrain was investigated based on the Williamson-Hall plot. Crystallinity, shape and size of the nanoparticles were studied using high resolution transmission electron microscopy and high resolution scanning electron microscopy. Brunauer-Emmet-Teller measurement revealed that the sample has high surface area of 116 m^2/g. Barrett-Joyner-Halenda test showed that the sample is mesoporous. The magnetization was found to increase from 66.5 ± 0.3 emu/g to 84.4 ± 0.5 emu/g from 300 K to 4 K, respectively. Furthermore, the electrochemical sensing properties of $Ba_{1/3}Mn_{1/3}Co_{1/3}Fe_2O_4$ nanoparticles were investigated using cyclic voltammetry. A glassy carbon electrode was modified using the synthesized $Ba_{1/3}Mn_{1/3}Co_{1/3}Fe_2O_4$ nanoparticles. The modified electrode demonstrated excellent electrocatalytic activity towards didanosine, an anti-HIV drug. A linear response to the drug concentration was obtained in the range 0.001 to 5.0 µM with a detection limit of 1.0 nM. The electrode was highly stable, reproducible and was successfully used to determine trace amounts of didanosine in human urine samples.

1 Introduction

Nanomaterials have actively emerged as an area of interest among researchers because of their distinctive physical and chemical properties, such as high surface area, catalytic effect and mass transport due to quantum size effect.[1] Recent years have witnessed an upsurge in the exploration of spinel nanoferrites (SNPs) for their useful magnetic and electrical properties for technological applications in diverse fields such as ferrofluids, magneto-optics, spintronics, medical diagnostics, information storage systems, microwave absorbers and manufacturing anodes for batteries.[2] The magnetic properties of SNPs can be tuned by substituting different elements at their sub-lattices.[3] Several factors, such as purity, homogeneity and microstructure, are known to affect the magnetic properties of these ferrites.[4] A number of methods for synthesis of SNPs have been reported. Some of these methods are hydrothermal, co-precipitation, electrospinning, sol-gel, combustion and conventional ceramic techniques.[5] However, the easiness and higher control of particle sizes by wet chemistry methods make them preferable, as compared to solid state reaction techniques.[6] SNPs have also been found to exhibit advantages towards electrochemical detection of a wide range of analytes due to their distinctive electrical and catalytic properties.[7,8] Research is in progress to improve their electrochemical sensing ability to the maximum possible extent. Adding dopant to ferrites is shown to vary their electronic conductivity, thus extending its application in the field of electroanalysis.[9] In the present work, we have synthesized novel single phase spinel structured

[a] School of Chemistry and Physics, Westville campus, University of KwaZulu-Natal, P/Bag X5401, Durban 4000, South Africa.
[b] Department of Pharmaceutical Chemistry, Discipline of Pharmaceutical Sciences, College of Health Sciences, University of KwaZulu-Natal, Durban 4000, South Africa

[1] All the authors contributed equally to this article.
Corresponding authors: nadir-shams@hotmail.com
Karpoormath@ukzn.ac.za

$Ba_{1/3}Mn_{1/3}Co_{1/3}Fe_2O_4$ nanoparticles and investigated the structure and properties of the nanomaterial obtained. The presence of magnetic ions in the sample has led us to investigate its magnetic properties. Literature survey reveals that iron-based magnetic nanoparticles act as excellent materials for electrode modification in electroanalysis owing to their unique properties such as large surface area and high surface energy.[10,11] Magnetic nanoparticles have also been found to function as electron-conducting pathways allowing rapid transfer of electrons between the redox system and the electrode surface.[12,13] This information motivated us to study the electrochemical properties of the newly synthesized magnetic $Ba_{1/3}Mn_{1/3}Co_{1/3}Fe_2O_4$ nanoparticles. The work further investigates the electrochemical sensing ability of the synthesized nanoparticles towards didanosine (DDI), an anti-HIV drug.

Didanosine (2',3'-dideoxyinosine, DDI) (Scheme 1) is a purine nucleoside analogue, which is used to treat human immunodeficiency virus (HIV) infection as part of highly active antiretroviral therapy (HAART).[14] Approved in 1991 by the Food and Drug Administration (FDA), it belongs to a class of antiretroviral drugs called nucleoside reverse transcriptase inhibitors (NRTIs).[15] Adverse effects of the drug include peripheral neuropathy, pancreatitis, retinal changes, optic neuritis and lactic acidosis.[16] Determination of DDI is very important for quality control and obtaining the optimal therapeutic drug concentration. A number of analytical methods have been reported for the estimation of the drug, with the majority of them involving high-performance liquid chromatography and spectrophotometric techniques, which are expensive as well as time-consuming.[17-20] Due to their high sensitivity, specificity, low cost of instrumentation and simplicity, the electroanalytical methods have proved to be expedient for quantitative analysis of several drugs in bulk, pharmaceutical formulations and biological fluids. However, to date, very few voltammetric methods have been reported for DDI determination. Ozoemena *et al.*[21] fabricated electrochemical sensors, based on metallopthalocyanine (MPc, M = Co, Fe) complexes impregnated carbon paste electrode to determine the drug. Later, Farias *et al.*[22] developed an adsorptive stripping method for the quantification of DDI at a mercury film electrode. Metal ferrite nanoparticles show promising application in the field of electroanalysis.[7] Hence, in the present study, a novel electrochemical sensor based on the $Ba_{1/3}Mn_{1/3}Co_{1/3}Fe_2O_4$ nanoparticles modified glassy carbon electrode was developed for sensitive determination of DDI. The electrochemical behavior of the drug was studied using cyclic voltammetry (CV) and the modified electrode was validated for quantification of the drug in human urine samples.

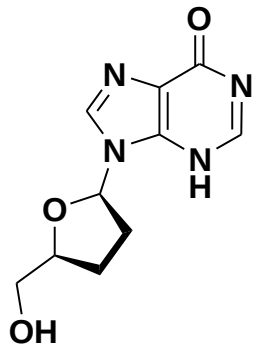

Scheme 1 Chemical structure of didanosine.

2 Experimental

$Ba_{1/3}Mn_{1/3}Co_{1/3}Fe_2O_4$ nanoparticles were synthesized by the glycol-thermal method in a Watlow series model PARR 4843 stirred pressure reactor. The starting materials ($BaCl_2.6H_2O$: 99%, $MnCl_2.6H_2O$: 99%, $CoCl_2.4H_2O$: 98% and $FeCl_2.6H_2O$: 99%) were purchased from Sigma-Aldrich. Stoichiometric metal chlorides were dissolved in deionized water using a magnetic stirrer for 30 minutes. Drops of NH_4OH were added slowly to the mixture, until a pH of 9 was

reached. The precipitate was washed using deionized water over a Whatman glass microfiber filter. A standard solution of silver nitrate was used to confirm that all the chloride ions had been removed. The wet precipitate was reacted in ethylene glycol at 200 °C in a pressure reactor under continuous stirring for 6 hours, at a pressure of about 100 Psi. After the reaction, the mixture was washed with deionized water and finally with ethanol. The final product was dried using a 200 W infra-red lamp. The powder was homogenized using an agate mortar and pestle. The phase and structural characterization of the sample was conducted using a Phillips X-ray diffractometer (Model: PANalytical, EMPYREAN) using CoKα radiation ($\lambda = 1.7903$ Å). The morphology and micro-structure of the nanoparticles were investigated by high-resolution transmission electron microscope (HRTEM) (Jeol_JEM-1010) and high-resolution scanning electron microscope (HRSEM) (Ultra Plus ZEISS-FEG HRSEM instrument). The textural and porosity properties of the nanoparticles were investigated using micrometrics tristar II 3020 instrument, with liquid N_2 as the analysis gas. A mini cryogen free magnetization measurement system (Cryogenic Ltd, UK) was used to perform low temperature magnetization measurements from 4 to 300 K within magnetic fields of up to 5 Tesla.

For the electrochemical experiments, DDI and potassium ferricyanide were obtained from Sigma-Aldrich, USA. All other chemicals used were of analytical reagent grade and purchased from Merck. A stock solution (2.00×10^{-3} M) of DDI was prepared in double distilled water and stored in a dark place, when not in use. Phosphate buffer solution (PBS; μ = 0.2 M) at various pH values was used as supporting electrolyte. Pure nitrogen gas was purged into the DDI containing solution for atleast 3 minutes before each experiment. The electrochemical measurements were performed on an electrochemical analyzer (Model 800B Series, CH Instruments, Inc.) and conducted in a single-compartment three-electrode glass cell, which consisted of a reference electrode (Ag/AgCl), a counter electrode (platinum wire) and a working electrode (a bare/modified glassy carbon electrode). For sample preparation, the urine samples (obtained from laboratory personnel) were diluted 100 times by phosphate buffer of pH 7.2. The dilution process helps in reducing the matrix effect.[23] The drug was then quantified in spiked human urine samples using CV**.**

Before fabrication of the modified electrode, the glassy carbon electrode (GCE) was cleaned by polishing with 0.05 micron alumina slurry on a polishing cloth for about 30 seconds. The electrode was then rinsed thoroughly with double-distilled water and dried in air. A 0.5 mg/mL suspension of $Ba_{1/3}Mn_{1/3}Co_{1/3}Fe_2O_4$ nanoparticles in dimethyl formamide was prepared. 10.0 μL of the suspension was then cast onto the cleaned electrode surface and dried to constitute $Ba_{1/3}Mn_{1/3}Co_{1/3}Fe_2O_4$/GCE. The active surface area of bare and modified GCE was measured by recording CVs in 1.0 mM $K_3[Fe(CN)_6]$ solution at different scan rates and using the Randles-Sevcik equation.[24] The active surface area was found to be 0.070 cm^2 and 0.218 cm^2 for bare GCE and $Ba_{1/3}Mn_{1/3}Co_{1/3}Fe_2O_4$/GCE, respectively.

3 Results and discussion

In the present work, $Ba_{1/3}Mn_{1/3}Co_{1/3}Fe_2O_4$ nanoparticles were successfully synthesized using glycol thermal route. The structure, morphology, magnetic and electrochemical properties of the sample was investigated by XRD, HRTEM, HRSEM, magnetization and voltammetry measurements, respectively.

3.1 Characterization of $Ba_{1/3}Mn_{1/3}Co_{1/3}Fe_2O_4$ nanoparticles

Fig. 1 depicts X-ray powder diffraction (XRD) patterns of $Ba_{1/3}Mn_{1/3}Co_{1/3}Fe_2O_4$ nanoparticles. The XRD shows a well-defined spinel structure with no impurity peaks. The lattice parameter a was calculated using Bragg's equation, where d is the inter-planar spacing and hkl are the Miller indices. The average crystalline size was determined using Scherrer's equation, where β is

the full-width at half-maximum of the most intense (311) XRD peak and θ is the Bragg's angle.[25] The microstrain was determined using Williamson-Hall plot, as displayed in Fig. 2. The distribution of the data points reflects the homogeneity of the microstrain. The lattice parameter, crystallite size and microstrain for the as-prepared $Ba_{1/3}Mn_{1/3}Co_{1/3}Fe_2O_4$ nanoparticles were found to be 0.839±0.003 nm, 8.37± 0.06 nm and 0.0015±0.0001, respectively.

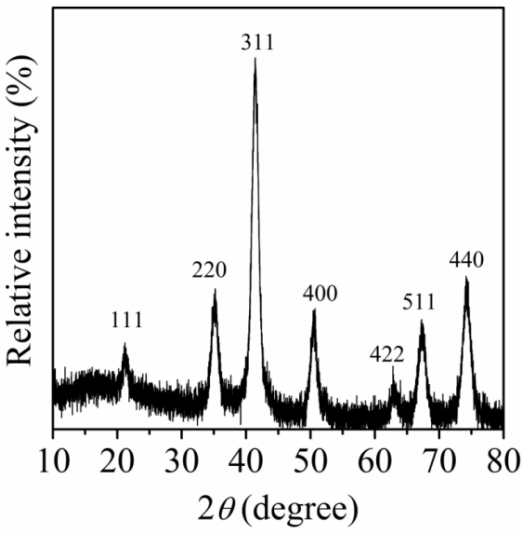

Fig.1 X-ray diffraction pattern for the synthesized $Ba_{1/3}Mn_{1/3}Co_{1/3}Fe_2O_4$ nanoparticles.

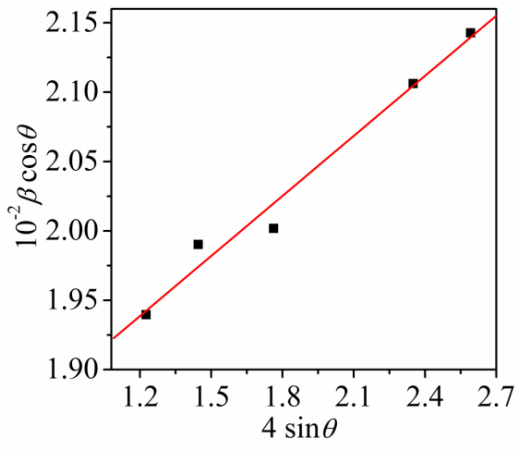

Fig. 2 Plot of βcosθ versus 4Sinθ for the synthesized $Ba_{1/3}Mn_{1/3}Co_{1/3}Fe_2O_4$ nanoparticles.

Fig. 3 exhibits images of the as-prepared $Ba_{1/3}Mn_{1/3}Co_{1/3}Fe_2O_4$ nanoparticles, captured via high resolution transmission electron microscopy (HRTEM) and high resolution scanning electron microscopy (HRSEM). The images in (Fig. 3A and 3B) show quasi-spherical like shapes. Mono-dispersive characteristic was observed. The lattice fringes are well-defined (as seen in Fig. 3A), thus the particles exhibit well-formed crystalline structure. The marked d spacing of 0.252 nm is anticipated to reflect 311 planes. The average particle sizes are found to be 9.3±2 nm. Fig. 3C shows that the particles are well-dispersed. The HRTEM and HRSEM images in Fig. 3 are support the XRD result in term of crystallinity and size of the synthesized nanoparticles.

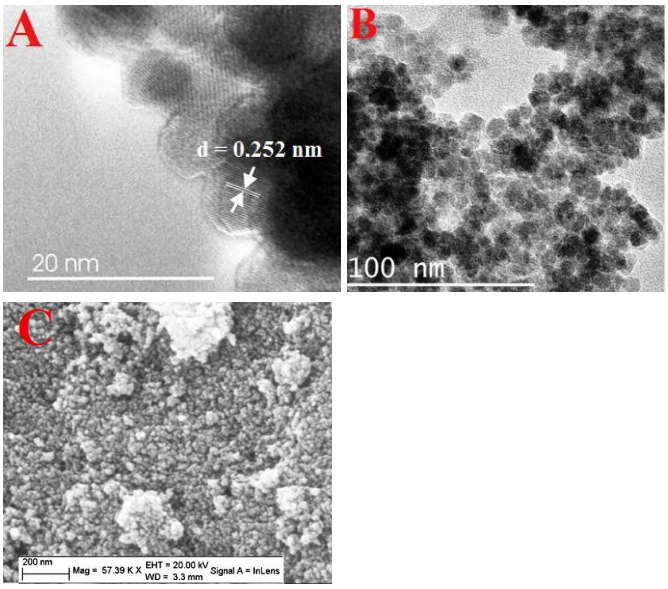

Fig. 3 HRTEM with 20 nm magnification (A), HRTEM with 100 nm magnification (B), and HRSEM (C) image for the synthesized $Ba_{1/3}Mn_{1/3}Co_{1/3}Fe_2O_4$ nanoparticles.

The sample revealed high surface area of 116 m^2/g, as deduced from Brunauer-Emmet-Teller (BET) surface area measurement. The texture and character of the pores were studied using isothermal N_2 adsorption-desorption measurement. Fig. 4 shows N_2 gas adsorption isotherms for the as-prepared $Ba_{1/3}Mn_{1/3}Co_{1/3}Fe_2O_4$ nanoparticles. The

adsorption of N_2 increased to a maximum value of 222 cm^3/g at a relative pressure (P/P_0) of 99%, whilst desorption of the gas decreased to a lowest value of 19 cm^3/g, as the P/P_0 decrease to 0.01%. The adsorption and desorption curves were found to merge, indicating that the hysteresis loop is associated with the N_2 condensation inside the sample pores.[26] The hysteresis loop can be classified into type IV isotherm, which suggests the mesoporous property of the sample.[27] Barrett-Joyner-Halenda (BJH) measurement was carried out to explore the scattering of pores. Most of the scatter points were placed in the range between 2-47 nm, further confirming the mesoporous property of the nanoparticles.[28] Since the distribution peak of the pores was sharp (as demonstrated in the inset of Fig. 4), it indicates homogeneous pore distribution.

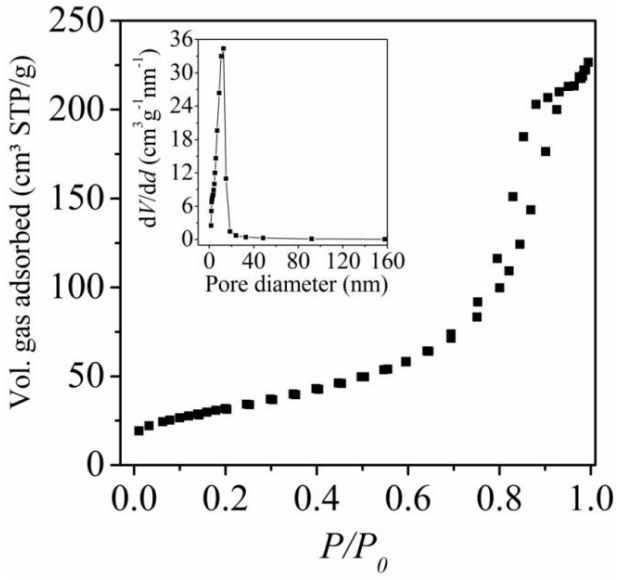

Fig. 4 N_2 gas adsorption isotherms for the as-prepared $Ba_{1/3}Mn_{1/3}Co_{1/3}Fe_2O_4$ nanoparticles. The inset shows the pore size distribution.

Fig. 5 depicts *M-H* loops at different measuring temperatures for the as-prepared $Ba_{1/3}Mn_{1/3}Co_{1/3}Fe_2O_4$ nanoparticles. The measurements were achieved in external magnetic fields in the range -5 T to +5 T. The results show an increase in the magnetization from 66.5±0.3 emu/g to 84.4±0.5 emu/g, as the measuring temperature decreased from 300 K to 4 K, respectively. The coercivity increased from 0.009 ± 0.004 T to 1.010 ± 0.004 T with decrease in temperature from 300 K to 4 K, respectively. The significant increase in the coercivity value with decrease in the measuring temperature indicates that the sample becomes magnetically harder at low temperature, which is related to the spin freezing effect. Also, the sample shows a distortion in the hysteresis loops at low temperature (as seen in Fig. 5). This distortion is anticipated to be due to the combined effect of soft and hard magnetic phases. The spin disorder in the surface layer is also expected to lead to such behavior.[29]

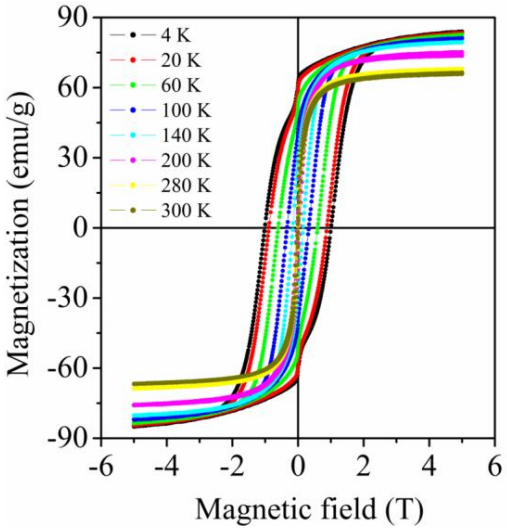

Fig. 5 Hysteresis loops measurements at different temperature for as-prepared $Ba_{1/3}Mn_{1/3}Co_{1/3}Fe_2O_4$ ferrite nanoparticles.

The approach to saturation of the magnetization (M) was used to obtain the values of $M_S(T)$ as a function of the measuring temperature. Fig. 6 exhibits the initial magnetization curves for the as-prepared $Ba_{1/3}Mn_{1/3}Co_{1/3}Fe_2O_4$ nanoparticles. The best fitting curves (in red), obtained for the initial magnetization curves of the sample, are based on the empirical law of approach to saturation magnetization, $M = M_S(T)[1-\frac{a}{H}-\frac{b}{H^2}]+\chi H$, where χ is the high-field susceptibility and the

parameters, a and b, are constants.[30] The magnetic parameters (maximum magnetization, saturation magnetization, coercivity, remanent magnetization and the squareness of the hysteresis loop) of the as-prepared $Ba_{1/3}Mn_{1/3}Co_{1/3}Fe_2O_4$ nanoparticles are summarized in Table 1.

Table 1 Maximum magnetizations at 5 T (M_m), saturation magnetizations obtained from empirical law of approach to saturation (M_S), coercive fields (H_C), remanent magnetizations (M_r) and squareness of the hysteresis loops (M_r/M_S) for the $Ba_{1/3}Mn_{1/3}Co_{1/3}Fe_2O_4$ nanoparticles.

T (K)	M_m (emu/g) ±0.5	M_S (emu/g) ±0.1	H_C (T) ±0.004	M_r (emu/g) ±1	M_r/M_S
4	84.4	90.5	1.010	60	0.716
10	84.1	90.4	0.948	60	0.659
20	83.8	90.2	0.886	59	0.650
40	83.5	89.6	0.742	55	0.614
60	82.5	88.7	0.599	51	0.573
80	82.3	87.7	0.461	46	0.522
100	81.6	86.7	0.325	39	0.483
120	80.5	85.1	0.211	32	0.372
140	79.8	84.0	0.153	26	0.309
180	77.0	80.4	0.066	14	0.169
200	75.1	78.5	0.042	8	0.100
240	71.8	74.9	0.042	5	0.069
280	68.3	72.9	0.010	4	0.075
300	66.5	67.6	0.009	4	0.071

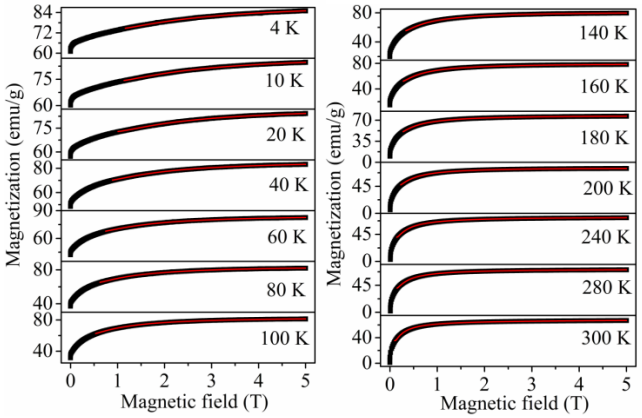

Fig. 6 Initial magnetization curves at different temperature for as-prepared $Ba_{1/3}Mn_{1/3}Co_{1/3}Fe_2O_4$ nanoparticles.

The values of the remanent magnetization (M_r) and the squareness of the hysteresis loops M_r/M_S were found to increase dramatically with decrease in temperature. As reported in the literature, M_r values depend on magnetic anisotropy, particle microstructure as well as stress sensitivity.[31] Fig. 7 shows that the decline in M_r is related to the reduction in magnetic anisotropy strength. The inset in Fig. 7 displays the variation of M_r/M_S with change in temperature. It is observed that as the temperature increases, M_r/M_S monotonically decreases. Based on Stoner–Wohlfarth theory, the value of M_r/M_S for cubic and uniaxial anisotropy was found to be 0.832 and 0.5, respectively.[32] At low temperature (T<80 K), the values of M_r/M_S were much higher than 0.5, as can be seen in the inset of Fig. 7, suggesting that at low temperature the as-prepared $Ba_{1/3}Mn_{1/3}Co_{1/3}Fe_2O_4$ nanoparticles tend to have cubic magnetocrystalline anisotropy.

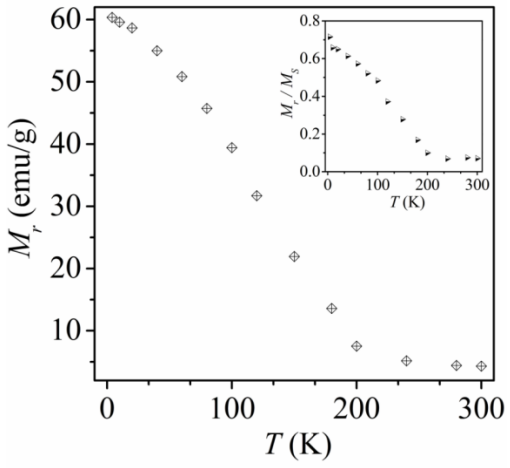

Fig. 7 Variation of the remanent magnetization (M_r) plotted as a function of the measuring temperature. The inset shows the variation of the reduced remanent magnetization (M_r / M_S) with measuring temperature of $Ba_{1/3}Mn_{1/3}Co_{1/3}Fe_2O_4$ nanoparticles.

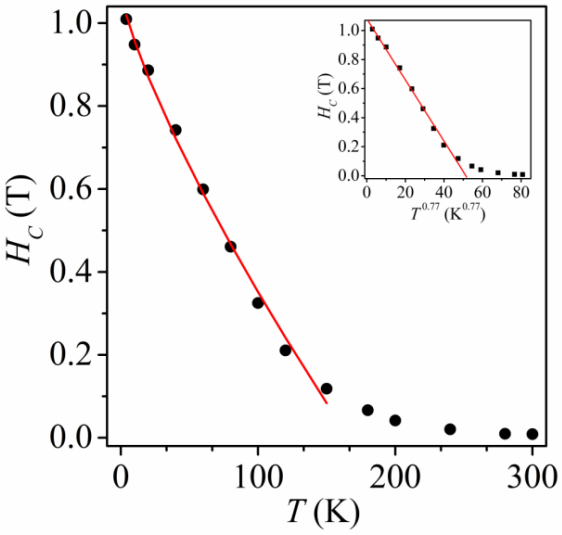

Fig. 8 Coercivity temperature dependency for the as-prepared $Ba_{1/3}Mn_{1/3}Co_{1/3}Fe_2O_4$ nanoparticles. The red line in the inset shows the $T^{0.77}$ dependence.

Fig. 8 depicts the variation of the coercivity (H_C) as a function of the measuring temperature. Significant increase in H_C was observed at temperatures lower than 200 K. This was associated with the thermal oscillation of blocked moments through the anisotropy barrier.[33] The temperature dependence of H_C for non-interacting mono-domain particles in the temperature range below the blocking temperature T_B, is described by Kneller's law $H_C(T) = H_C(0)[1-(T/T_B)^{\alpha}]$, where $H_C(0)$ is the coercivity at 0 K, and α is a constant.[34] For modified Kneller's law, the value of α is 0.5. The H_C was found to follow T^{α} law with $\alpha = 0.77$, as reported by Pfeiffer *et al.*[35] The collected data of H_C as a function of measuring temperature was plotted and a correlation coefficient of 0.9955 was obtained. The value of $H_C(0)$, T_B and α were found to be 1.08±0.03 T, 166±5 K and 0.77±0.07, respectively. The inset in Fig. 8 demonstrated the variation of H_C with $T^{0.77}$ for the as-prepared $Ba_{1/3}Mn_{1/3}Co_{1/3}Fe_2O_4$ nanoparticles.

For ferromagnetic and ferrimagnetic systems, the temperature dependence of magnetization is associated with the spin waves (magnons), where the magnetization decreases with increase in the measuring temperature. The thermal behavior of the magnetization is usually described by Bloch's law $M_S(T) = M_S(0)[1-(T/T_0)^{\beta}]$, where $M_S(0)$ is the saturation magnetization at 0 K, T_0 is the temperature at zero magnetization, $1/T_0$ is Bloch's constant that depends on the nanoparticle structure and β is the Bloch's exponent.[36] This model is effective for bulk systems with β of 3/2. For the nano-scale materials, the magnons with wavelength larger than the particle size (due of finite size effect) need thermal energy in order to be excited. Thus, the modified Bloch's law with β value greater than 3/2 is expected to be an appropriate model to describe such a system. As seen in Fig. 9, the temperature dependence of magnetization is fitted in accordance with the modified Bloch's law with a correlation coefficient of 0.9995. The values of $M_S(0)$, T_0 and β, determined from the fitting curves, are 90.5±0.1 emu/g, 704±10 K and 1.62±0.02, respectively.

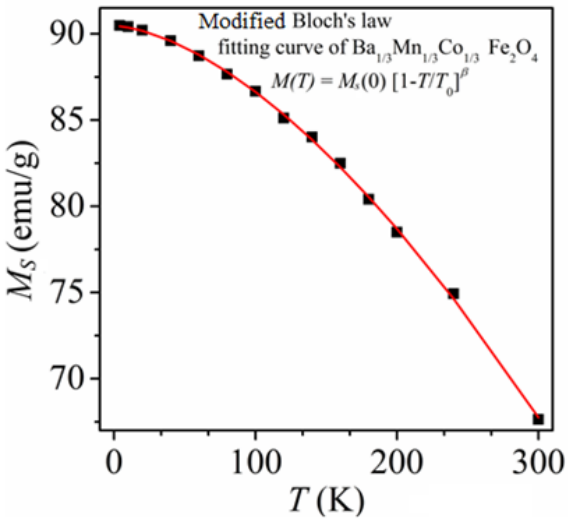

Fig. 9 Thermal dependency of saturation magnetization for the as-prepared $Ba_{1/3}Mn_{1/3}Co_{1/3}Fe_2O_4$ nanoparticles. (The red line shows the fit curve according to modified Bloch's law.)

3.2 Electrochemical behavior towards didanosine

3.2.1 Electrochemical activity

The electrochemical activity of the synthesized $Ba_{1/3}Mn_{1/3}Co_{1/3}Fe_2O_4$ nanoparticles towards DDI was investigated using CV. Fig. 10 depicts cyclic voltammograms recorded for 0.5 µM DDI in 0.1 M PBS (pH 7.2) at bare GCE and $Ba_{1/3}Mn_{1/3}Co_{1/3}Fe_2O_4$/GCE. No voltammetric peak was observed at the bare electrode. However, the voltammetric response improved significantly at the modified electrode, exhibiting a distinct peak at 0.75 V. This electrocatalytic activity of the $Ba_{1/3}Mn_{1/3}Co_{1/3}Fe_2O_4$/GCE is attributed to the unique properties of the synthesized nanoparticles and the large surface area of the electrode. Since the electrode is modified with transition metal nanoparticles, it is anticipated that when an electrochemical reaction takes place, these transition metal ions function as active sites[37], acting as catalyst for the oxidation of DDI. Hence, $Ba_{1/3}Mn_{1/3}Co_{1/3}Fe_2O_4$/GCE demonstrated enhanced electrochemical sensing property as compared to the bare GCE.

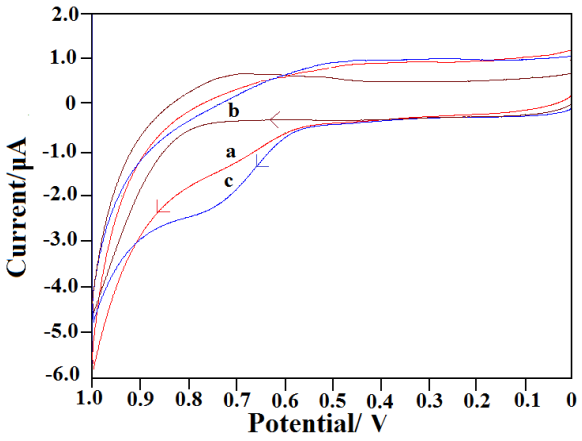

Fig. 10 Typical cyclic voltammograms observed (a) in absence of DDI at $Ba_{1/3}Mn_{1/3}Co_{1/3}Fe_2O_4$/GCE and in presence of 0.5 µM DDI at (b) bare GCE and (c) $Ba_{1/3}Mn_{1/3}Co_{1/3}Fe_2O_4$/GCE in 0.1 M PBS (pH 7.2) at a scan rate of 100 mV/s.

3.2.2 Effect of scan rate and pH

The effect of scan rate (v) on the electrochemical behavior of DDI at $Ba_{1/3}Mn_{1/3}Co_{1/3}Fe_2O_4$/GCE was investigated in the range from 10-200 mV/s. The peak current (i_p) was found to increase linearly with an increase in v (as seen in Fig. 11 (A)), indicating that the electrooxidation of DDI on the modified electrode is a typical adsorption-controlled process.[38] The relationship between i_p and v is expressed by the equation $i_P(\mu A) = 0.0087v + 0.1239$, with a correlation coefficient of 0.9967. Further, log i_p was plotted against $\log v$ (Fig. 11 (B)) and a linear relationship, expressed by the equation $\log i_P = 0.8089 \log v - 1.6004$ having a correlation coefficient of 0.9937, was obtained. A slope of 0.8 was observed, which is close to the theoretical value of 1.0 expected for an ideal adsorption-controlled electrode process.[39] This confirmed that the electrooxidation of DDI was adsorption-controlled. The peak potential (E_p) was also observed to shift towards more positive values with an increase in v, suggesting the irreversible nature of the electrochemical process.[40]

On plotting E_p versus $\log v$ (Figure 11 (C)), a straight line was observed that followed the equation $E_P = 0.0681 \log v + 0.6134$, with a

correlation coefficient of 0.9995. For an irreversible electron transfer, the E_p is expressed by the Laviron's equation,

$$E_P = E^{0'} + \left(\frac{2.30RT}{\alpha nF}\right)\log\left(\frac{RTk^0}{\alpha nF}\right) + \left(\frac{2.30RT}{\alpha nF}\right)\log v$$

where $E^{0'}$ is the formal redox potential, n is the number of electrons transferred in the electrochemical process, α is the electron transfer coefficient, k^0 is the standard heterogeneous rate constant of the reaction, and the other mentioned symbols have their usual meanings.[41] The value of αn is calculated from the slope of E_p versus $\log v$ plot. In the given system, the slope was found to be 0.0681 V. Considering R = 8.314 J/K mol, F = 96480 C/mol and T = 298 K, αn was found to be 0.87. The value of n was then calculated using the equation $\alpha = \frac{47.7}{E_p - E_{p/2}}$, where $E_{p/2}$ is the half-peak potential.[42] The value of n was found to be 1.64 (~2), indicating the involvement of two electrons in the oxidation of DDI at $Ba_{1/3}Mn_{1/3}Co_{1/3}Fe_2O_4$/GCE.

The pH of the supporting electrolyte exhibits significant influence on the electrooxidation of DDI at the modified electrode. Fig. 11 (D) depicts the effect of pH on E_p of 0.5 µM DDI using $Ba_{1/3}Mn_{1/3}Co_{1/3}Fe_2O_4$/GCE in 0.1 M PBS in the pH range 3.1-9.0. It was observed that as the pH value of the solution increased, the E_p shifted linearly towards less positive potentials, with a slope of 54.2 mV/pH. This value was close to the theoretical value of 59 mV/pH, indicated for electrochemical processes involving same number of electrons and protons.[43] Hence, it is suggested that two electrons and two protons participate in the electrooxidation of DDI, and the anticipated reaction mechanism is depicted in Scheme 2.

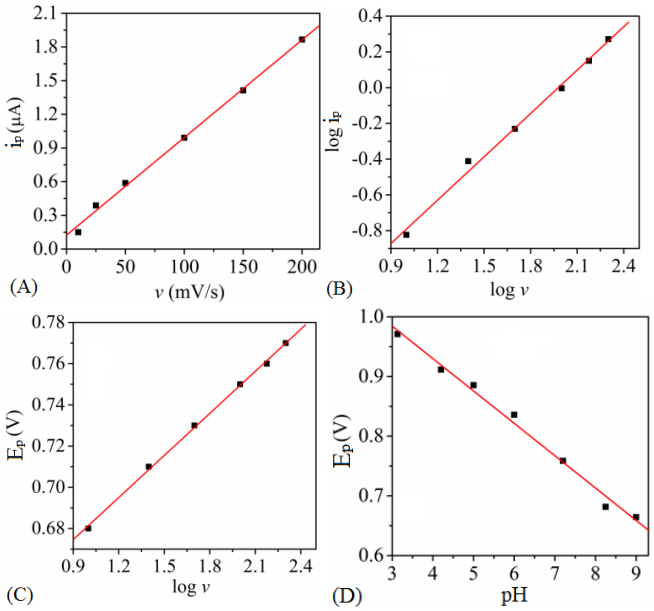

Fig. 11 (**A**) Observed dependence of peak current on scan rate; (**B**) Variation of the logarithm of peak current with the logarithm of scan rate; (**C**) Plot of E_p versus logarithm of scan rate; and (**D**) Dependence of E_p on pH for 0.5 µM DDI in 0.1 M PBS.

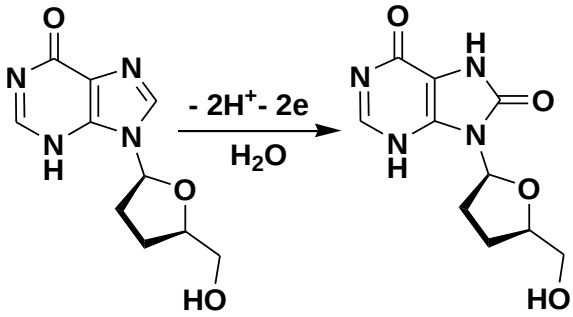

Scheme 2 Proposed electro-oxidation mechanism of DDI.

3.2.3 Analytical performance

Cyclic voltammograms of DDI with varied concentrations were recorded at $Ba_{1/3}Mn_{1/3}Co_{1/3}Fe_2O_4$/GCE under optimum experimental conditions. The oxidation peak current (peak height) was found to increase linearly with DDI concentration in the range 1.0×10^{-9} M to 5.0×10^{-6} M (as depicted in Fig. 12). The observed linear equation was

$i_p(10^{-6}\,\mathrm{A}) = 2178.6C$ (R^2 = 0.9989), where *C* is the concentration of DDI (in mM). The detection limit (LOD) was found to be 1.0 nM.

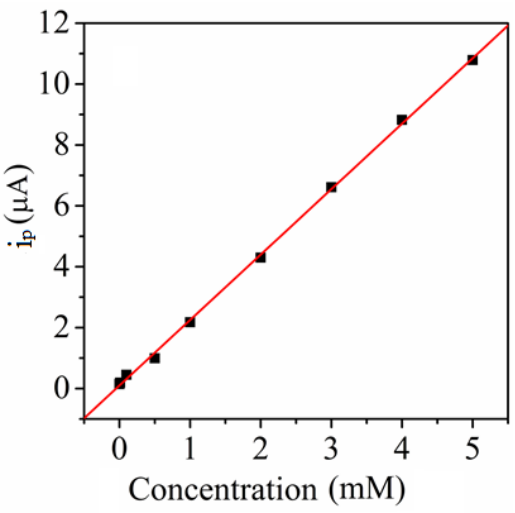

Fig. 12 Calibration plot observed for DDI at $Ba_{1/3}Mn_{1/3}Co_{1/3}Fe_2O_4$/GCE at pH=7.2.

The reproducibility and stability of $Ba_{1/3}Mn_{1/3}Co_{1/3}Fe_2O_4$/GCE was also investigated. A series of five modified electrodes were fabricated using the same procedure and then used for the determination of 0.5 µM DDI in 0.1 M PBS. A relative standard deviation (RSD) of i_p values recorded at the five electrodes was found to be 4.2%, suggesting good fabrication reproducibility of the proposed electrode. For six successive determinations of 0.5 µM DDI solution at the same modified electrode, the calculated RSD was 3.6%. Also, the CV response of $Ba_{1/3}Mn_{1/3}Co_{1/3}Fe_2O_4$/GCE was investigated for the same DDI concentration, after leaving the electrode unused for seven days. The peak potential did not exhibit any change and the peak current response also showed insignificant variation, suggesting good stability of the modified electrode. The selectivity of $Ba_{1/3}Mn_{1/3}Co_{1/3}Fe_2O_4$/GCE towards determination of 0.5 µM DDI was examined in the presence of organic species commonly present in real samples. The tolerance limit was fixed at the concentration of interfering species exhibiting a signal change of 5% or more. It was found that over 10-fold excess concentration of ascorbic acid, dopamine and uric acid did not interfere with the voltammetric response of DDI, suggesting good selectivity of the method.

In order to evaluate the analytical applicability of the proposed method, assays were performed in two human urine samples. The samples were spiked with varying quantities of DDI and the recovery study of the drug was conducted. The observed results (summarized in Table 2) show satisfactory recoveries, thus validating that the proposed method has good accuracy. Fig. 13 displays the cyclic voltammogram obtained for DDI spiked human urine sample (sample 1), where a peak is observed at 0.75 V that refers to the presence of DDI. An additional peak is observed at ~0.4 V, which is attributed to the existence of uric acid in the urine sample, suggesting that the biological substances present in urine did not show any interference in determination of the drug. Hence, the method can be used efficiently for quantification of DDI in real matrices.

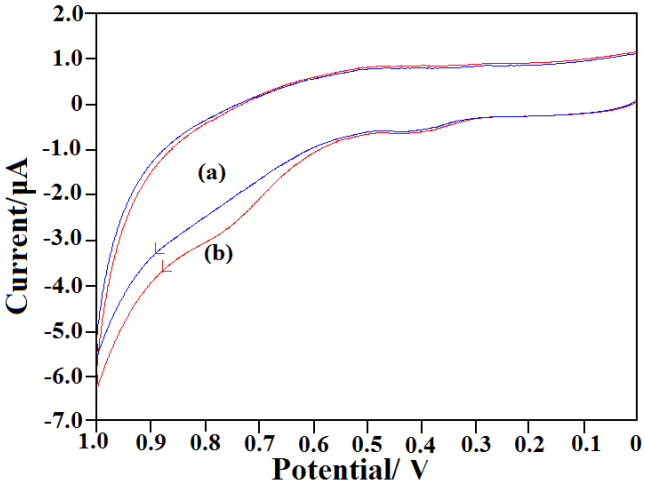

Fig. 13 Cyclic voltammograms of (a) blank urine sample 1 and (b) urine sample 1 spiked with 0.5 µM standard solution of DDI, under optimum experimental conditions.

Table 2 Recovery results obtained for DDI in human urine sample at $Ba_{1/3}Mn_{1/3}Co_{1/3}Fe_2O_4$/GCE.

Sr. No.	Added (M)		Found (M)		Recoveries (%)	
	Sample 1	Sample 2	Sample 1	Sample 2	Sample 1	Sample 2
1	1.00×10^{-9}	1.00×10^{-9}	9.91×10^{-10}	1.01×10^{-9}	99.1	101.0
2	1.00×10^{-8}	1.00×10^{-8}	9.84×10^{-9}	9.92×10^{-9}	98.4	99.2
3	1.00×10^{-7}	1.00×10^{-7}	9.87×10^{-8}	1.01×10^{-7}	98.7	101.0
4	5.00×10^{-7}	5.00×10^{-7}	4.96×10^{-7}	5.04×10^{-7}	99.2	100.8
5	1.00×10^{-6}	1.00×10^{-6}	1.01×10^{-6}	1.02×10^{-6}	101.4	102.3

4 Conclusions

The present work reports simultaneous substitution of Ba, Mn and Co into ferrite spinel structure using glycol thermal method. The spinel phase structure of the sample was identified using X-ray powder diffraction technique. The microstrain was estimated from Williamson-Hall plot, with the scattered data showing homogeneity in the sample microstrain. High-resolution transmission electron microscopy and high-resolution scanning electron microscopy were used to monitor the morphology of the as-prepared $Ba_{1/3}Mn_{1/3}Co_{1/3}Fe_2O_4$ nanoparticles. The results show mono-dispersive crystallite particles having high value surface area as deduced from Brunauer-Emmet-Teller testing. The sample was found to possess mesoporous character, as observed from Barrett-Joyner-Halenda measurement. The magnetization investigation revealed that the sample tends to become magnetically harder at low temperature. The spontaneous magnetization increased with decrease in temperature. The remanent magnetization and reduced remanent magnetization values were also found to increase with decrease in the measuring temperature. Temperature dependence of coercivity and magnetization were observed to follow Kneller's and modified Bloch's law, respectively. The electrocatalytic activity of the synthesized nanoparticles was investigated by fabricating $Ba_{1/3}Mn_{1/3}Co_{1/3}Fe_2O_4$ nanoparticles modified glassy carbon electrode as a voltammetric sensor towards didanosine. The modified electrode, with advantages such as simple fabrication procedure, excellent reproducibility, wide linear concentration range and significantly low detection limit, was successfully applied for the quantification of the drug in human urine samples, thus offering a promising substitute to the commonly reported chromatographic and spectrophotometric methods for quantification of didanosine.

Acknowledgements

The authors would like to thank the National Research Foundation (NRF) of South Africa for VSM and mini cryogen free measurement equipment grants, Department of Pharmaceutical Chemistry (College of Health Sciences, University of KwaZulu-Natal, South Africa) for financial support (NT) and Sudan University of Science and Technology for the study leave (NSEO).

References

1 G. B. H. Sohn and R. E. Cohen, Chem. Mater., 1997, 9, 264-269.
2 C. Vazquez-Vazquez, M. A. Lopez-Quintela, M. C. Bujan-Nunez and J. Rivas, J. Nanopart. Res., 2011, 13, 1663-1676.
3 R. K. Gopathi, V. K. Katrapally and V. Y. Chetty, Mat. Sc. Appl., 2012, 3, 87-91.
4 Y. Purushotham, M. Singh, S. P. Sud and P. V. Reddy, Int. J. Mod. Phys. B, 1998, 12, 2247-2262.
5 M. P. Reddy, X. Zhou, A. Yann, S. Du, Q. Huang and A. M. A. Mohamed, Superlatt. Microstr., 2015, 81, 233-242.
6 S. Diodati, L. Nodari, M. M. Natile, U. Russo, E. Tondello, L. Lutterotti and S. Gross, Dalton Trans., 2012, 41, 5517-5525.
7 V. A. Kumary, J. Divya, T. E. M. Nancy and K. Sreevalsan, Int. J. Electrochem. Sc., 2013, 8, 6610-6619.
8 A. A. Ensafi, F. Saeid, B. Rezaei and A. R. Allafchian, Anal. Methods, 2014, 6, 6885-6892.
9 B. Ul-ain, S. Ahmed, M. A. ur Rehman, Y. Huang and C. A. Randall, New J. Chem., 2013, 37, 2768-2777.
10 M. Hasanzadeh, N. Shadjou, Nasrin, M. de la Guardia, Tr. Anal. Chem., 2015, 72, 1-9.

11 G. Absalan, M. Akhond, A. Bananejad, H. Ershadifar, J. Iran. Chem. Soc., 2015, 12, 1293-1301.
12 D. Grieshaber, R. MacKenzie, J. Vörös, Sensors, 2008, 8, 1400-1458.
13 H. Wei, E. Wang, Luminescence, 2011, 77-85.
14 B. Roca, C. Lapuebla and B. Vidal-Tegedor, Int. J. Infect. Dis., 2005, 9, 195-200.
15 B. A. Ahidjo, R. Veale, A. G. Duse, P. Becker and E. Marais, Int. J. Antimicrob. Agents, 2008, 32, 186-191.
16 C. E. Reust, Am. Fam. Physician, 2011, 83, 1443-1451.
17 A. M. C. de Oliveira, T. C. R. Loewen, L. M. Cabral, E. M. dos Santos, C. R. Rodrigues, H. C. Castro and T. C. dos Santos, J. Pharm. Biomed. Anal., 2005, 38, 751-756.
18 H. Sura, S. Bonthu and T. E. G. K. Murthy, J. Adv. Pharm. Edu. Res., 2013, 3, 187-195.
19 R. N. Kane, P. S. Bhokare, C. C. Nalawade, M. S. Sayyed and R. D. Paliwal, Int. J. Pharm. Chem. Sc., 2012, 1, 2277-5005.
20 J. N. Sangshetti, P. A. Kulkarni and D. B. Shinde, Tr. App. Sc. Res., 2007, 2, 71-75.
21 K. I. Ozoemena, R. I. Stefan-van Staden and T. Nyokong, Electroanal., 2009, 21, 1651-1654.
22 P. A. M. Farias, A. A. Castro and A. I. P. Cordoves, J. Electrochem. Sci. Eng., 2012, 2, 133-142.
23 M. M. I. Khan, A. M. J. Haque and K. Kim, J. Electroanal. Chem., 2013, 700, 54-59.
24 R. O. Kadara, N. Jenkinson and C. E. Banks, Sens. Act. B: Chem., 2009, 138, 556-562.
25 S. Sutradhar, K. Mukhopadhyay, S. Pati, S. Das, D. Das and P. K. Chakrabarti, J. Alloys Comp., 2013, 576, 126-133.
26 C. P. Bean and J. D. Livingston, J. Appl. Phys., 1959, 30, 120S-129S.
27 M. Kruk and M. Jaroniec, Chem. Mater., 2001, 10, 3169-3183.
28 P. B. Lihitkar, S. Violet, M. Shirolkar, J. Singh, O. N. Srivastava, R. H. Naik and S. K. Kulkarni, Mater. Chem. Phys., 2012, 133, 850-856.
29 R. H. Kodama, C. L. Seaman, A. E. Berkowitz and M. B. Maple, J. Appl. Phys., 1994, 75, 5639-5641.
30 J. Liu, W. Ren, D. Li, N. Sun, X. Zhao, J. Li and Z. Zhang, Phys Rev B, 2007, 75, 064429/1-064429/5.
31 G. F. Dionne, Proc. IEEE, 1975, 63, 777-789.
32 E. C. Stoner and E. P. Wohlfarth, Trans. Roy. Soc., 1948, A240, 599-644.
33 K. Maaz, A. Mumtaz, S. K. Hasanain and M. F. Bertino, J. Magn. Magn. Mater., 2010, 322, 2199-2202.
34 K. Maaz, S. Karim, K. J. Lee, M. H. Jung and G. H. Kim, Mater. Chem. Phys., 2012, 133, 1006-1010.
35 H. Pfeiffer and W. Schueppel, Phys. Status Solidi A., 1990, 119, 259-269.
36 R. H. Kodama J. Magn. Magn. Mater, 1999, 200, 359-372.
37 D. Ye, Y. Xu, L. Luo, Y. Ding, Y. Wang and X. Liu, J. Solid State Electrochem., 2012, 16, 1635-1642.
38 E. Laviron, A. Vallat and R. Maunier-Prest, J. Electroanal. Chem., 1994, 379, 427-435.
39 D. K. Gosser, in Cyclic Voltammetry: Simulation and Analysis of Reaction Mechanisms, VCH, New York, 1993, pp. 43.
40 J. I. Gowda and S. T. Nandibewoor, Asian J. Pharm. Sc., 2014, 9, 42-49.
41 E. Laviron, J. Electroanal. Chem., 1979, 101, 19-28.
42 A. J. Bard and L.R. Faulkner, in Electrochemical methods: Fundamentals and applications (2nd ed.), Wiley, New York, 2004, pp. 236.
43 L. Fotouhi, M. Fatollahzadeh and M. M. Heravi, Int. J. Electrochem. Sci., 2012, 7, 3919-3928.

Graphical Abstract

Investigation of magnetic and electrochemical sensing properties of novel $Ba_{1/3}Mn_{1/3}Co_{1/3}Fe_2O_4$ nanoparticles

Nadir S.E. Osman, Neeta Thapliyal, Thomas Moyo and Rajshekhar Karpoormath

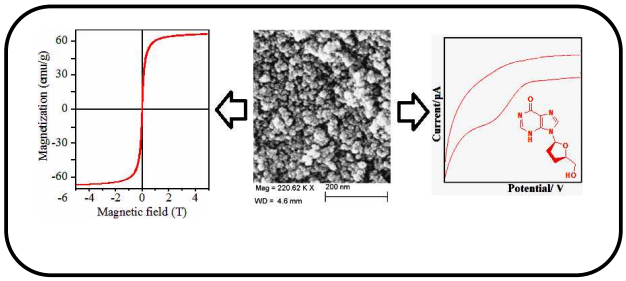

Novel $Ba_{1/3}Mn_{1/3}Co_{1/3}Fe_2O_4$ nanoparticles were successfully synthesized followed by their characterization and investigation of their magnetic and electrochemical sensing properties.